

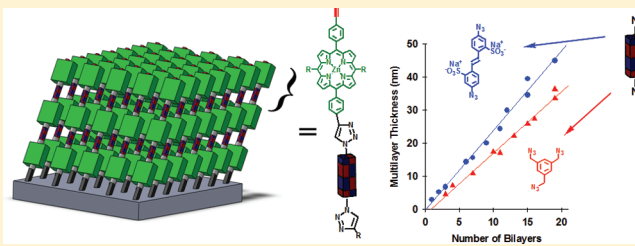
## Thickness, Surface Morphology, and Optical Properties of Porphyrin Multilayer Thin Films Assembled on Si(100) Using Copper(I)-Catalyzed Azide–Alkyne Cycloaddition

Peter K. B. Palomaki, Alexandra Krawicz, and Peter H. Dinolfo\*

Department of Chemistry and Chemical Biology and The Baruch '60 Center for Biochemical Solar Energy Research, Rensselaer Polytechnic Institute, 110 8th Street, Troy, New York 12180, United States

 Supporting Information

**ABSTRACT:** We report the structure, optical properties and surface morphology of Si(100) supported molecular multilayers resulting from a layer-by-layer (LbL) fabrication method utilizing copper(I)-catalyzed azide–alkyne cycloaddition (CuAAC), also known as “click” chemistry. Molecular based multilayer films comprised of 5,10,15,20-tetra(4-ethynylphenyl)porphyrinzinc(II) (**1**) and either 1,3,5-tris(azidomethyl)-benzene (**2**) or 4,4'-diazido-2,2'-stilbenedisulfonic acid disodium salt (**3**) as a linker layer, displayed linear growth properties up to 19 bilayers. With a high degree of linearity, specular X-ray reflectivity (XRR) measurements yield an average thickness of 1.87 nm/bilayer for multilayers of **1** and **2** and 2.41 nm/bilayer for multilayers of **1** and **3**. Surface roughnesses as determined by XRR data fitting were found to increase with the number of layers and generally were around 12% of the film thickness. Tapping mode AFM measurements confirm the continuous nature of the thin films with roughness values slightly larger than those determined from XRR. Spectroscopic ellipsometry measurements utilizing a Cauchy model mirror the XRR data for multilayer growth but with a slightly higher thickness per bilayer. Modeling of the ellipsometric data over the full visible region using an oscillator model produces an absorption profile closely resembling that of a multilayer grown on silica glass. Comparing intramolecular distances from DFT modeling with experimental film thicknesses, the average molecular growth angles were estimated between 40° and 70° with respect to the substrate surface depending on the bonding configuration.



### INTRODUCTION

The fabrication of thin films utilizing layer-by-layer (LbL) assembly techniques provides a straightforward and flexible method for the creation of nanostructured materials with excellent precision. The LbL approach allows for facile manipulation of physical, electronic, photophysical, and chemical properties of the thin films. Films with well-defined structures have successfully been made utilizing the LbL technique and their properties are generally dictated by the polymeric or molecular components used in the assembly process. This flexibility in thin film design has significant implications in the development of advanced materials for nonlinear optics, photovoltaics, memory devices, sensors, molecular electronics, etc.<sup>1–3</sup>

LbL based thin film structures are unique among self-assembled systems in that they provide control over the nanoscopic ordering of the materials with respect to a macroscopic orientation, i.e., the axis normal to substrate surface. The most common variety of LbL assemblies are those based on the sequential deposition of polyanions and polycations on a charged substrate surface. These materials, initially described by Decher,<sup>4–6</sup> rely on the electrostatic interactions between the opposite charges on the different polyelectrolytes and have resulted in the construction of a wide range of nanostructured thin film architectures.<sup>1–3,7</sup>

Numerous variations of the LbL assembly scheme have also been developed utilizing discrete molecular species as the layer components. Molecular based LbL methodologies, also known as molecular layer deposition (MLD), typically employ self-limiting reactions between symmetric multifunctional molecules and linkers that yield single monolayers deposited at each step. Sagiv was the first to describe molecular-based LbL assemblies using siloxane couplings between layers of alkane chains.<sup>8,9</sup> Following these reports, Mallouk described the use of zirconium phosphonates as an efficient coupling group for the creation of mixed inorganic–organic multilayers with efficient growth over several multilayers.<sup>10–14</sup> Since these first reports of molecular based LbL assemblies, others have expanded on the siloxane<sup>15–21</sup> and zirconium (or hafnium) phosphonates,<sup>22–26</sup> as well as using additional organic<sup>1,27–31</sup> and inorganic<sup>32–35</sup> coupling chemistries as a means of multilayer formation. Generally, these types of reaction sequences have been shown to produce well ordered, multilayer thin films that are amenable to various molecular components.

**Received:** November 11, 2010

**Revised:** February 14, 2011

**Published:** March 16, 2011

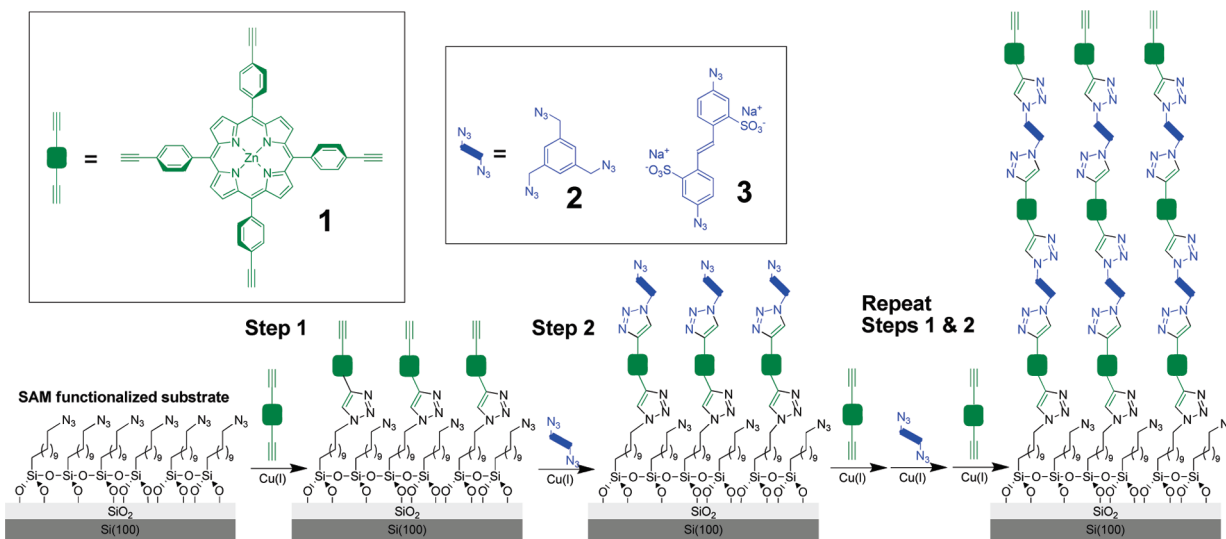


**Figure 1.** Schematic representation of the CuAAC based LbL formation of molecular multilayer thin films on Si(100) substrates and the molecular components used throughout this work.

In an effort to provide even greater flexibility in terms of the molecular species that can be incorporated into the thin film materials, we recently developed a new LbL methodology that employs copper(I)-catalyzed azide–alkyne cycloaddition (CuAAC) reactivity, commonly referred to as “click” chemistry.<sup>36</sup> Following its discovery by Sharpless<sup>37</sup> and Meldal<sup>38</sup> in 2001, CuAAC has gained significant popularity in recent years for a variety of synthetic and materials applications due to its simplicity, versatility, and high yield for the isomerically pure 1,4-triazole.<sup>39,40</sup> The use of CuAAC to covalently modify surfaces was first described by Collman and Chidsey, who employed azido terminated alkane thiols and ethynyl substituted redox probes to functionalize Au(111) electrode surfaces.<sup>41–44</sup> These Au(111) electrodes coated with mixed azido-alkane self-assembled monolayers provide a highly tunable substrate to which a wide variety of ethynyl substituted molecules could be attached. Subsequent studies have extended this surface modification technique to include oxide surfaces through the use of azido-alkylsiloxane SAMs.<sup>45–48</sup>

Our extension of this surface modification technique to molecular based LbL assemblies is outlined in Figure 1.<sup>36</sup> While CuAAC has been used to build triazole-linked polymer<sup>49–51</sup> and dendrimer<sup>52</sup> based multilayers, it has not, to our knowledge, been used to assemble molecular multilayers prior to our report.<sup>36</sup> The initial step involves the modification of an oxide substrate (ITO, silica glass, etc.) with an alkyl siloxane self-assembled monolayer (SAM) to provide the initial attachment point. Following this step, a multiethynyl functionalized molecule, such as porphyrin 1, is reacted with the surface using CuAAC chemistry to generate a molecular monolayer covalently attached through 1,4-triazole linkages. The resulting ethynyl terminated surface is then reacted with a multiazido molecule (termed a “linker” from here on), such as 2 or 3, to regenerate an azido-rich surface. These two self-limiting reactions are then repeated sequentially to generate the desired number of molecular bilayers. The choice of 1 as our primary molecular building block was initially made based on its relative ease of synthesis, multiple ethynyl functionalities, and high extinction coefficient that allows for the straightforward monitoring of multilayer growth through absorption measurements. The highly tunable

optical and electrical properties of porphyrins have led them to be of significant importance in a range of materials chemistry applications.<sup>53</sup> The inclusion of porphyrin based molecular building blocks, such as 1, into multilayer films could lead to a wide range of applications including artificial photosynthetic processes,<sup>54–56</sup> semiconductor sensitization,<sup>57–59</sup> sensors,<sup>54–56</sup> and catalysts.<sup>63–65</sup>

Molecular multilayer thin films grown on silica glass and ITO using 1 and 2 or 3 showed highly linear absorbance growth trends through 10s of bilayers and alternating surface properties as probed by water contact angle. Additionally, polarized absorbance measurements indicated the presence of some molecular ordering of the porphyrins with respect to surface normal. Preliminary specular X-ray reflectivity (XRR) results suggest a growth of 2.47 nm/bilayer for multilayers containing 1 and 3 on a glass substrate.<sup>36</sup> Herein we expand on these results by examining the thickness, surface morphology, and optical properties of thin films made by a CuAAC LbL technique on Si(100) through the use of specular XRR, tapping mode atomic force microscopy (AFM), spectroscopic ellipsometry, and UV–visible specular reflectance spectroscopy.

## RESULTS

**Multilayer Growth and UV–Visible Specular Reflectance Spectroscopy.** Molecular multilayer growth on Si(100) substrates was achieved in an analogous method as described previously for silica and indium tin oxide (ITO).<sup>36</sup> The method requires an azido-terminated SAM attached to the substrate surface as a starting point. Here, we use a 11-azidoundecyltrimethoxysilane hydrolyzed on the native oxide of Si(100). Multilayer formation starts with the attachment of one layer of ethynyl porphyrin (1) via CuAAC chemistry (Figure 1, step 1). Under the reaction conditions described previously and herein, a dense monolayer of 1 is covalently attached to the azido SAM, yielding a surface that is now terminated with ethynyl groups. This is then followed with a multiazido linker layer (2 or 3) again using CuAAC chemistry (Figure 1, step 2) to create one molecular bilayer and regenerating an azido terminated surface. Steps 1 and 2 are repeated sequentially to create the desired number of molecular bilayers.

The high molar absorptivity of tetraphenyl porphyrins allows us to track multilayer growth with UV-visible absorption spectroscopy. To monitor the absorbance profile of these films on nontransparent substrates (i.e., silicon), we have employed specular reflectance spectroscopy techniques at a near normal incidence angle. The spectra resulting from the Fresnel reflectivity of 1 through 19 bilayers of **1** and **3** is shown in the bottom panel of Figure 2. Instead of the normal absorption profile for tetraphenylporphyrins, the reflectivity spectrum of these samples show a first-derivative like line shape, with increased reflectance on the high energy side of the absorption features resulting from the classic Kramers-Kronig effect.<sup>66</sup> The top panel of Figure 2 shows the absorption profile (transmission mode) from a multilayer grown with the same molecular components on silica glass.<sup>36</sup> Despite the convolution due to the Kramers-Kronig effect on the reflectance spectra, two Q-band features around 560 and 605 nm as well as the large Soret peak at 440 nm are clearly observed and they increase in intensity (decreasing reflectivity) with an increase in the number of bilayers. The spectra consistently decrease in reflectivity as each bilayer is added to the silicon substrate. Similar trends in reflectivity changes were observed for multilayers formed with **1** and **2** (see Supporting Information, Figure S1).

**X-ray Specular Reflectivity.** X-ray specular reflectivity (XRR) has been used previously to probe the height, roughness, and density of multilayer thin-film materials grown using LbL assembly techniques.<sup>16,23,32,67,68</sup> X-rays impinging on a thin-film will reflect off of the upper air-film and lower film-substrate interfaces resulting in an interference pattern as the angle of incidence is changed. The dependence of the position of the interference patterns or Kiessig fringes<sup>69</sup> on thickness is given by the following Bragg equation modified for index of refraction<sup>23,67</sup>

$$n\lambda = 2d(\theta_n^2 - \theta_c^2)^{1/2} \quad (1)$$

In eq 1,  $d$  is the film thickness,  $\theta_n$  is the position of the  $n$ th fringe, and  $\theta_c$  is the critical angle for the film. The thickness of a thin film can be found using this equation by plotting  $\theta_n^2$  vs  $n^2$  where the slope will equal  $\lambda^2/4d^2$ . A more comprehensive analysis involves fitting of the XRR profiles to a model that is based on the electron density profile of the thin film perpendicular to the substrate surface. This is done via eq 2 where  $R(q_z)$  is the Fresnel reflectivity of the thin film sample,  $R_f(q_z)$  is the ideal Fresnel reflectivity of the Silicon substrate,  $\rho_{Si}$  is the electron density of silicon,  $\rho(z)$  is the electron density profile of the thin-film and  $q_z$  is the wave transfer vector ( $q_z = (4\pi/\lambda) \sin \theta$ ).<sup>70,71</sup>

$$\frac{R(q_z)}{R_f(q_z)} = \left| \frac{1}{\rho_{Si}} \int \frac{\partial \rho(z)}{\partial z} e^{-izq_z} dz \right|^2 \quad (2)$$

Figure 3a shows the XRR curves resulting from multilayers of **1** and **3** grown on a Si(100) substrate (open circles). The interference patterns increase in frequency and shift to lower  $q_z$  (and lower  $\theta$ ) as the number of bilayers and thickness of the films increase. The attenuation of the fringe patterns at higher  $q_z$  (or  $\theta$ ) is a result of the roughness of the films along with the limitations of the instrument. Fitting of the XRR curves was performed using the LEPTOS software suite from Bruker AXS where a layered sample model was constructed to generate a simulated reflectivity curve (solid lines) based on eq 2. The model consisted of four simulated layers: (1) bulk Si(100), (2) a thin film of SiO<sub>2</sub> to represent the native oxide surface, (3) an alkane self-assembled monolayer, and (4) the porphyrin based multilayer structure. We found it necessary to include an oxide

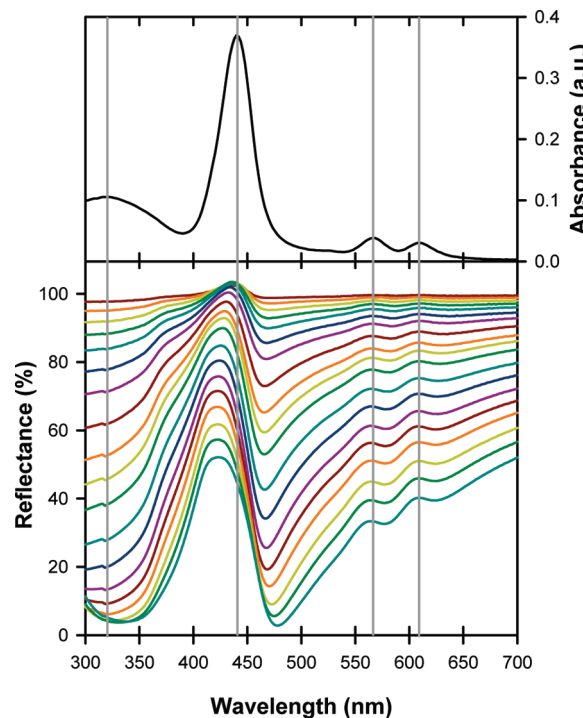


**Figure 2.** Top: UV-visible absorption profile (transmission mode) for 10 bilayers of **1** and **3** assembled on glass modified with 11-azidoundecyltrimethoxysilane (data adapted from a previous report).<sup>36</sup> Bottom: UV-visible specular reflectivity profiles of 1 through 19 bilayers of **1** and **3** on Si(100) modified with 11-azidoundecyltrimethoxysilane.

layer in the model to achieve a good correlation between the raw data and fits. The solid lines in Figure 3a represent the best fits to the X-ray reflectivity data using this model.

Figure 3b shows the electron density profiles of the multilayer structures normalized to Si as a function of the distance ( $z$ ) from the substrate surface. The electron density drops sharply from that of Si to a local minimum as a result of the lower SAM density and then rises to that of the multilayer film which remains constant until the film/air interface, before dropping to zero. Throughout the XRR data fitting process, it was observed that the total organic film thickness (SAM and multilayer) was a robust variable and remained nearly constant when either the SAM or multilayer thicknesses were altered. XRR analysis of the 11-azidoundecyltrimethoxysilane SAM on Si(100) yielded 1.8 nm for the thickness and 0.85 g/cm<sup>3</sup> for the density (see the Supporting Information). These values resulted in the best data fits for the multilayer structures and were held constant for the remaining samples. The results of the XRR data fitting for all four sample sets are shown in Table S1. It is important to note that thicknesses of the multilayer films calculated manually using only the observed Kiessig fringe maxima via eq 1 were nearly identical to those obtained using the LEPTOS software.

Figure 4 shows the XRR derived multilayer thickness as a function of the number of bilayers for all samples examined. The thickness results obtained by XRR confirm the expectation that multilayers grown with different azido linker units (**2** and **3**) result in different thicknesses. The average thickness of multilayers grown using porphyrin **1** and linker **2** was found to be 1.87 nm/bilayer, whereas multilayers grown with **1** and **3** had an average thickness of 2.41 nm/bilayer ( $R^2 = 0.988$ ). It is important

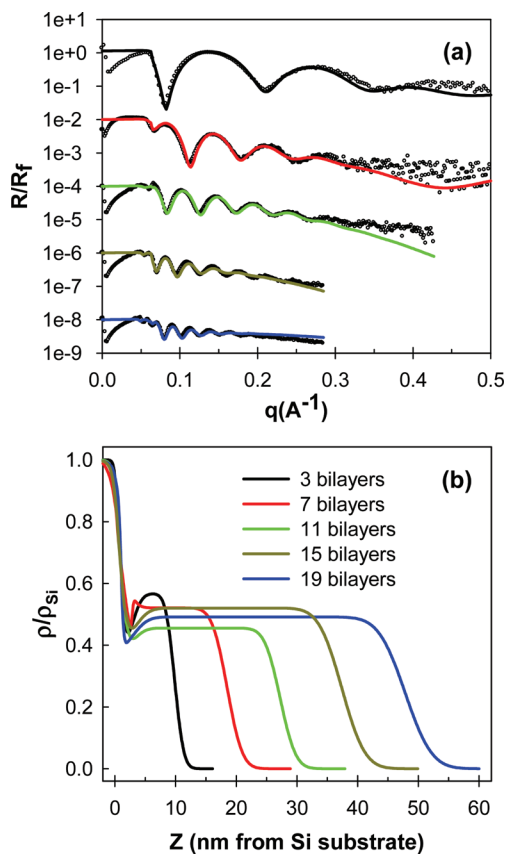


**Figure 3.** Panel A: Specular XRR of multilayers of 1 and 3 on Si(100) for the stilbene A sample set. Data are shown as open circles and the best fit models as solid lines (black, red, green, brown, and blue for 3, 7, 11, 15, and 19 bilayers, respectively). The data and fits are offset for clarity. Panel B: Electron density profiles normalized to Si as a function of distance away from the substrate surface for 3, 7, 11, 15, and 19 bilayers of 1 and 3. These profiles correspond to the best fits of the XRR data shown in panel A.

to note that for one sample set, multiple slides were grown in parallel using the same solutions and reaction times. Up to 7 separate samples were made in parallel and still resulted in a linear thickness trend:  $R^2 = 0.989$  for 1 and 2 and  $R^2 = 0.988$  for 1 and 3. This shows that CuAAC is a reproducible and robust method to build multilayer thin films.

As can be seen in Figure 3B, the interfacial roughness gives rise to the gradual changes in the electron density profile of the films. The roughness of the multilayer films generally increase with greater number of molecular bilayers. This is apparent in the gradual change from a near vertical electron density profile at the film/air interface (3 bilayers, black) to a more gradual sloping profile for the final 19 bilayer sample (blue). The roughness at the multilayer/air interface as determined by XRR fitting is shown versus the number of bilayers in Figure 5 for all samples used in this study. There is a clear trend of increasing surface roughness with an increase in the number of bilayers, most likely due to the dendritic nature of the porphyrin used in this study (vide infra). Further work is underway to investigate the structure and morphology of films grown using different molecular components.

**Spectroscopic Ellipsometry.** Spectroscopic ellipsometry was employed as a secondary method to compare thicknesses and to determine the optical constants of the multilayer films. Ellipsometry has often been used in conjunction with XRR to determine thickness of nanometer scale thin films<sup>72–80</sup> and LbL

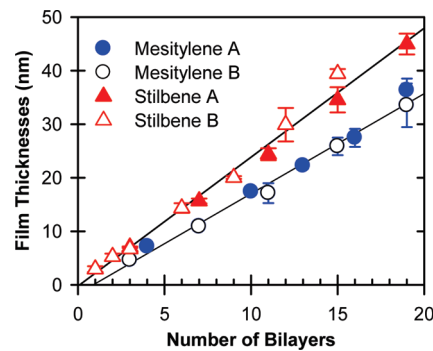


**Figure 4.** Multilayer film thicknesses of all samples determined by fitting of the XRR curves. Blue circles are multilayers constructed with porphyrin 1 and mesitylene linker 2, and red triangles are multilayers built with porphyrin 1 and stilbene linker 3. For both linkers two sample sets are differentiated by filled and open data symbols.

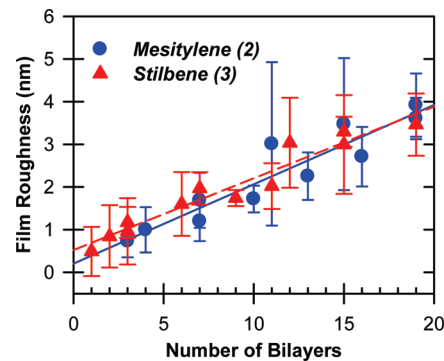


**Figure 5.** XRR determined roughness as a function of the number of bilayers (all data sets included). Samples grown with azido linker 2 are shown in blue circles and 3 in red triangles.

assemblies<sup>19,32,81–84</sup> on a variety of surfaces. Fewer examples employ spectroscopic ellipsometry to determine the optical constants,  $n$  and  $k$ , of the thin film materials over a wide spectral range.<sup>81,85</sup> To determine the multilayer thicknesses, ellipsometric incidence data,  $\Delta(\lambda)$  and  $\Psi(\lambda)$ , were collected at three angles of incidence ( $60^\circ$ ,  $65^\circ$ , and  $75^\circ$ ) and analyzed over the transparent region of the samples (where the extinction coefficient  $k(\lambda) \approx 0$ , from 673.9 to 741.5 nm, 10 data points) and fit using the Cauchy dispersion model that describes the refractive index ( $n$ ) as a function of the wavelength ( $\lambda$ ) via eq 3.<sup>86</sup>

$$n(\lambda) = A - \frac{B}{\lambda^2} - \frac{C}{\lambda^4} \quad (3)$$

Spectroscopic ellipsometry was performed on all multilayer samples following analysis by XRR. The data were fit using a three layer model consisting of (1) silicon substrate, (2) a thin layer of  $\text{SiO}_2$ , and (3) the multilayer film including the 11-azidoundecyltrimethoxysiloxane SAM. The  $\text{SiO}_2$  thickness was determined from an unfunctionalized Si(100) substrate cleaned in the same manner as the multilayer functionalized samples. Thickness values for the SAM-multilayer films are included in Table S1. Incorporation of a fourth layer to explicitly model the SAM did not significantly improve the quality of the fits. Typical values for A and B, determined by fitting the Cauchy dispersion model (eq 3) were found to be 1.45–1.91 and 0.01–0.14 for multilayers of 1 and 2 and 1.54–1.90 and 0.01–0.10 for

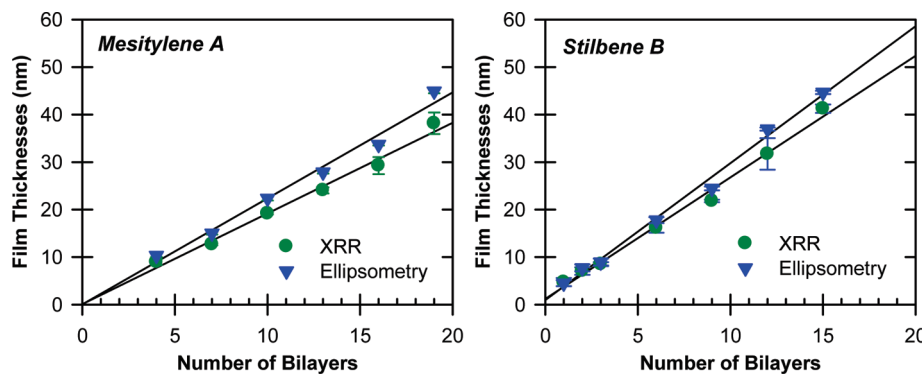


**Figure 6.** Comparison of film thicknesses as determined by XRR and ellipsometry for the mesitylene A and stilbene B sample sets. Notice the consistent difference between the two methods. 1.8 nm has been added to the XRR determined thickness values to account for the 11-azidoundecyltrimethoxysiloxane SAM in order to directly compare it to the ellipsometry data.

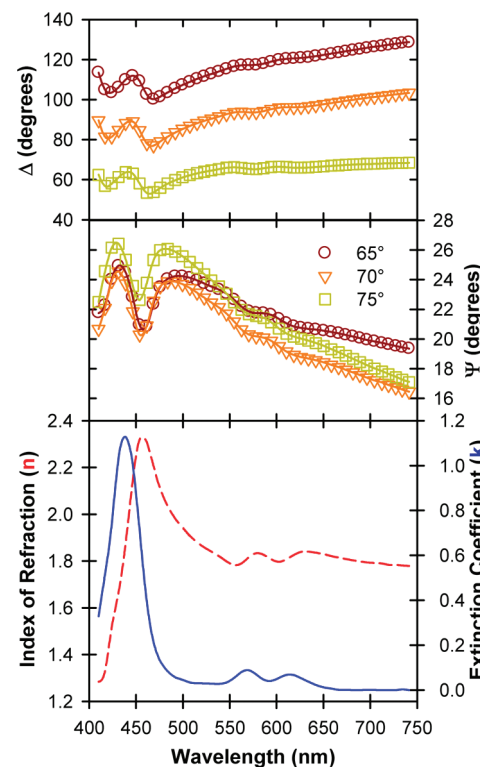
multilayers of **1** and **3**, respectively. The C term was found to have little influence on the data fitting and was set to 0 for all samples.

Figure 6 shows a comparison of the total SAM and multilayer film thickness for the mesitylene A and stilbene B samples sets as determined by XRR and spectroscopic ellipsometry. The ellipsometric film thicknesses mirror those determined by XRR, showing a linear growth trend over 19 bilayers, but are consistently higher by approximately 15%. Similar trends have been observed in other thin films where the ellipsometrically determined thicknesses are larger than thicknesses determined by XRR.<sup>19,72,76,79,80</sup> Notably, the variations in data with respect to the trend lines in Figure 6 are mirrored for almost all samples, suggesting a high degree of precision for the individual techniques but also the presence of systematic error of one or both techniques. Several people have pointed out that an accurate knowledge of  $n$  is required for correct thickness determination by ellipsometry, especially for ultrathin films.<sup>72,73,76,77,80</sup> Although we do not know the exact reason for the discrepancy between ellipsometrically and XRR determined thicknesses, we believe it may be in part due to inaccurate values of  $n$  for the multilayer films.

The spectroscopic analysis of these porphyrin based films at wavelengths shorter than 673 nm requires the use of a parametrized oscillator model to account for the absorption profile of the films and its effect on the complex index of refraction. The complex index of refraction ( $\tilde{n}$ ) is composed of the real refractive index ( $n$ ) and the imaginary part ( $ik$ ) according to the Kramers–Kronig relationship:<sup>85,86</sup>

$$\tilde{n}(\lambda) = n(\lambda) - ik(\lambda) \quad (4)$$

In this equation,  $k$  is extinction coefficient relating to the absorption profile of the multilayer films. The thicker samples were modeled using four Lorentzian oscillators to reconstruct the overall absorption profile of the porphyrin based multilayers (see Figure 2). A spectral deconvolution was performed on transmission absorption data for the analogous multilayers synthesized on silica glass (top spectra of Figure 2) and the resulting Lorentzian oscillator parameters were used as a starting point for spectroscopic ellipsometry data fitting where the film thickness was held constant at the values derived from the Cauchy layer modeling. Figure 7 shows the fits to the  $\Delta(\lambda)$  and  $\Psi(\lambda)$  data in the range of 410.0 to 741.5 nm (44 data points) and the resulting  $n$  and  $k$  profiles. The  $k$  profiles closely match that of the absor-



**Figure 7.** Spectroscopic ellipsometry data (410.0 to 741.5 nm, 44 data points) for 16 bilayers of **1** and **2** on Si(100) from the mesitylene A sample set. The top and middle panels show the  $\Delta$  and  $\Psi$  data (open symbols) and fits (solid lines) collected at an incident angle of 65, 70, and 75° (red circles, green squares, and orange triangles, respectively). The bottom panel shows the resulting optical constants for the multilayer film as determined by the oscillator model. The index of refraction ( $n$ ) is shown as the dashed red line and the extinction coefficient ( $k$ ) as the blue line.

ption profile for the porphyrin multilayers and the  $n$  spectra matches that of the specular reflectivity seen in Figure 2.

**Atomic Force Microscopy.** Several of the multilayer samples were also characterized by tapping mode atomic force microscopy (TM-AFM). For each of the multilayer sample sets, three representative samples were chosen: thinnest, middle, and thickest. Figure 8 shows  $1\text{ }\mu\text{m} \times 1\text{ }\mu\text{m}$  TM-AFM images collected for the Mesitylene A sample set. These are representative of

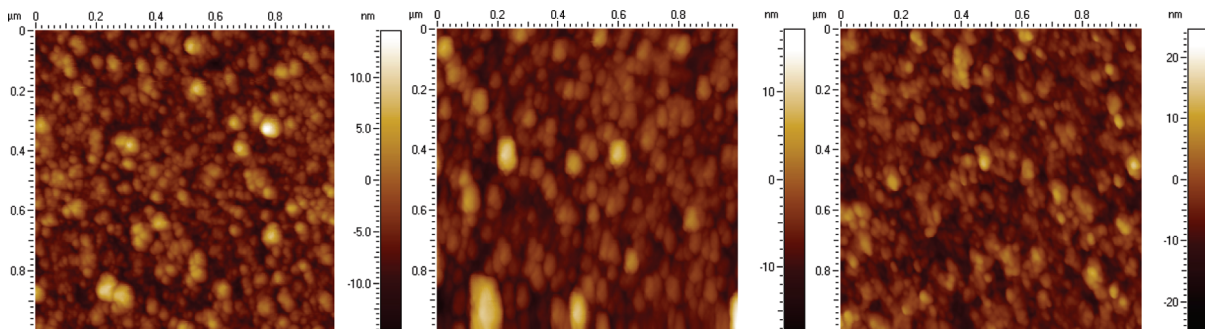


**Figure 8.** Representative AFM images from the mesitylene A sample set obtained in tapping mode with a  $1\text{ }\mu\text{m} \times 1\text{ }\mu\text{m}$  scan area. The left, middle and right images correspond to 4, 10, and 19 bilayers of **1** and **2** grown on Si(100), with calculated root mean squared roughness values of 3.4, 3.7, and 4.1 nm, respectively.

multilayer thin films for all samples shown in Table S1. Topography was analyzed focusing on the roughness trends that occur with increasing the number of deposited layers and the use of different linkers. Root-mean squared roughness ( $R_q$ ) of a cleaned Si(100) substrate was found to be on the order of 0.35 nm. The values of  $R_q$  for the images in Figure 8, for 4, 10, and 19 bilayers of **1** and **2** on Si(100) were 3.4, 3.7, and 4.1 nm, respectively. While these values are slightly higher than those determined from XRR data fitting, they are consistent across all samples (see values in Table S1). Larger area scans up to  $10\text{ }\mu\text{m} \times 10\text{ }\mu\text{m}$  reveal continuous multilayer films and similar roughness values.

**XPS Analysis of Cu Content of Multilayer Films.** X-ray photoelectron spectroscopy (XPS) was used to determine the concentration of copper catalyst remaining in the films after the multilayer fabrication process. Since no effort was made to remove the copper catalyst from the films other than simple solvent rinsing, we expected our films to contain measurable amounts of copper. Integration of the signals resulting from Cu  $2\text{p}_{3/2}$  and Zn  $2\text{p}_{3/2}$  allow us to quantify the amount of total copper with respect to zinc present in the samples (see the Supporting Information).<sup>87,88</sup> Films of **1** and **2** have a Cu:Zn ratio of 1.36:1, whereas films of **1** and **3** have a much lower ratio, 0.16:1. The surprisingly high amount of copper in the films made with stilbene linker **1** may be a result of the sulfonate groups present on linker **1**. We suspect that the sulfonate moieties sequester the copper catalyst causing it to remain in the film at high concentrations. The lack of a sodium peak in the XPS supports the conclusion that the Cu ions exchange with the sodium ions originally present on linker **1**. Azido linker **3** does not contain any chemical groups with a strong affinity for copper which may be the reason films grown using linker **3** have much lower levels of copper. Multilayer films made using CuAAC chemistry are likely to contain some amount of copper due to the ability of the basic nitrogen on the triazole ring to chelate copper. The ability of CuAAC modified surfaces to chelate copper ions has been suggested before.<sup>89</sup> We suspect that the triazole functionality causes the fixation of low levels of copper in films grown using linker **3** while the sulfonates are the major cause of the high levels of copper in films grown using linker **2**. It has been shown that EDTA is an effective Cu scavenger that can be used to remove copper from CuAAC functionalized films.<sup>89</sup> Further studies are underway to develop a method to remove the majority of copper from the multilayer structures during LbL formation.

## ■ DISCUSSION

The thickness results obtained by XRR and spectroscopic ellipsometry highlight the linearity and reproducibility in growth of multilayers up to 19 bilayers and across the 23 independent samples (see Figures 3 and 5). As determined by XRR, the thickness of multilayers grown with **1** and **2** was 1.87 nm/bilayer, and with **1** and **3** was 2.41 nm/bilayer. The thicknesses determined for multilayers of **1** and **3** was only slightly smaller than the value of 2.47 nm/bilayer for the same multilayers grown on silica glass as determined in our previous study.<sup>36</sup> As described above, the XRR results also show a steady increase in surface roughness with increasing number of bilayers. The XRR determined roughness values average approximately 12% of the film thickness for multilayers grown using both linkers (**2** and **3**). Similar thickness and roughness trends, deduced from a combination of XRR, AFM, and ellipsometry, have been observed for other porphyrin or phthalocyanine based multilayer films grown in a LbL fashion. Polyelectrolyte multilayer films consisting of nickel phthalocyanine tetrasulfonate poly(diallyldimethylammonium) chloride yielded thin film structures with linear growth trends up to a 27 bilayers and an increase XRR determined surfaces roughness that was approximately 5% of the film thickness. AFM analysis of the same films yielded roughness values that were approximately a factor of 2 larger, the difference being attributed to the different probing techniques.<sup>81</sup> AFM analysis of polyimide linked multi-porphyrin architectures grown on Si(100) surprising showed that thinner films were rougher than thicker, but still averaged between 10 and 20% of the overall multilayer thickness.<sup>30</sup> AFM determined surface morphology of uniform porphyrin based Zr-bisphosphonate multilayers films grown on Si and Au surfaces displayed substrate dependent roughnesses that ranged between 1 and 4 nm rms for three to five bilayers.<sup>55</sup>

Considering the size, number of azido groups, and differences in the rotational flexibility between the multiazido linkers (**2** and **3**) in our films, it is expected that the corresponding multilayer thicknesses should vary as well. In an effort to better understand the molecular orientation within the multilayer thin films we employed density functional theory to model the basic molecular building blocks to estimate the length of the repeat unit. The left side of Figure 9 shows the DFT-B3LYP optimized structures of **1** “clicked” with four pendant azido linker molecules (**1–2**<sub>4</sub> and **1–3**<sub>4</sub>). Due to the tetra-ethynyl functionality of **1** and triazido functionality of **2**, it is expected that several different bonding motifs could be present within these multilayer films. The right side of Figure 9 shows a schematic representation of the two

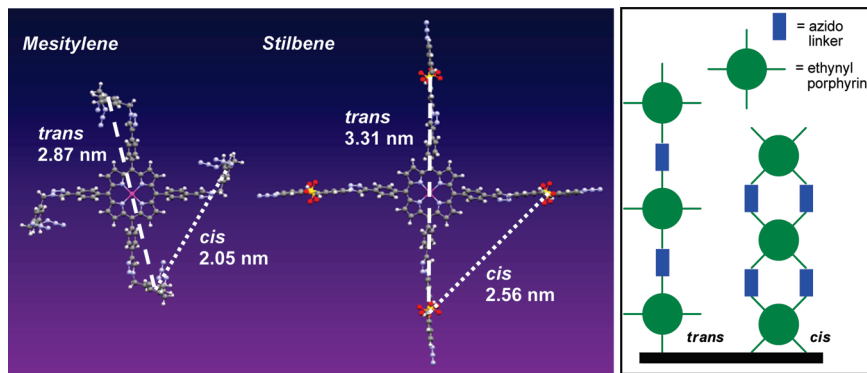


**Figure 9.** Left: DFT-B3LYP optimized structures of the individual repeat units for multilayer growth. Included with the optimized structures are relevant distances corresponding to the length of the repeat unit when considering trans (long dashed line) and cis (dotted line) bonding conformations within the multilayer structure. Right: Schematic representation of the two different possible modes of growth of the porphyrin multilayers (trans and cis).

**Table 1. Calculated Values of Molecular Repeat Units Length and Corresponding Growth Angles**

molecular components	bilayer thickness (nm)	repeat length (nm)		growth angle (deg)	
		trans	cis	trans	cis
1 and 2	1.87	2.87	2.05	40.7	65.8
1 and 3	2.41	3.31	2.56	46.7	70.3

different possible modes of growth of the porphyrin multilayers (trans and cis) representing the extremes of possible bonding configurations. The trans configuration assumes that each porphyrin utilizes only two of the four available ethynyl groups for multilayer growth, one on the top and one on the bottom, yielding the longest possible repeat unit. The cis configuration uses two ethynyl groups on each side of the porphyrin, resulting in the shortest possible repeat unit. Included with the optimized structures are relevant distances corresponding to the length of the repeat unit when considering trans (long dashed line) and cis (dotted line) bonding conformations within the multilayer structure. These distances are measured center-to-center between the azido linker units, corresponding to one repeat unit. Assuming that these two binding motifs represent the extremes of longest and shortest possible repeat units, we can calculate a range of average molecular orientations for the individual components. These values are shown in Table 1. Multilayers of **1** and **2** growing at 1.87 nm/bilayer give a range of molecular growth angles from 40.6° (trans) to 65.7° (cis) whereas films with **1** and **3** growing at 1.41 nm/bilayer are slightly higher at 46.7° (trans) to 70.2° (cis) with respect to the substrate surface. The real growth angles are probably within these ranges as the bonding motifs within the multilayer films are likely a mixture of both trans and cis.

The molecular building blocks used in this study were chosen to provide the best possible opportunity for linear LbL growth by providing multiple functional groups with CuAAC reactivity. The dendritic nature of **1** and **2** helps ensure that a maximal amount of terminal ethynyl and azide groups, respectively, are present at the surface of film following each molecular layer addition. This dendritic functionality may also lead to the increased roughness of the films as additional bilayers are added (see Figure 5). Attempts are currently underway in our laboratory to examine purely trans

disubstituted components in an effort to create multilayer films with lower roughness values.

## CONCLUSION

The structure, optical properties and surface morphology of two series of Si(100) supported molecular multilayers thin films assembled in a LbL fashion utilizing copper(I)-catalyzed azide–alkyne cycloaddition (CuAAC) reactivity has been reported. Molecular multilayers constructed using Zn(II) 5,10,15,20-tetra-(4-ethynylphenyl)porphyrin (**1**) and two azido-linker molecules (**2** and **3**) displayed linear growth trends up to 19 bilayers as determined by visible specular reflectance spectroscopy, XRR and spectroscopic ellipsometry. The difference in average bilayer thickness of the multilayers corresponds with variations in the intramolecular distances of the two azido linkers and triazole linked porphyrins as determined by molecular modeling. Due to the presence of multiple ethynyl and azido functional groups on **1** and **2**, there are several potential bonding configurations that may be present in the multilayer film leading to a range of possible growth angles of the molecular components. Comparing intramolecular distances from DFT modeling with experimental film thicknesses, the average molecular growth angles were estimated between 40° and 70° with respect to the substrate surface depending on the specific bonding configuration. Tapping mode AFM measurements confirm the continuous nature of the thin films with roughness values slightly larger than those determined from XRR and generally increase with the increasing number of bilayers in the film. Spectroscopic ellipsometry measurements utilizing a Cauchy model mirrors the XRR data for multilayer growth, but with a slightly higher thickness per bilayer. Modeling of the spectroscopic ellipsometry data over the full visible region using a Kramers–Kronig consistent oscillator model produces an absorption profile that closely resembles that of a multilayer grown on silica glass.

The CuAAC based LbL assembly technique provides a straightforward and flexible method for the construction of molecular multilayer thin films. The results described herein illustrate the reproducibility of this method in growing ordered and uniform thin films. This technique has the potential to provide a truly flexible method for the construction of nanostructured thin films with a variety of molecular components. While additional experiments are required to determine the scope and extent of this method, it is reasonable to assume that the

flexibility of the CuAAC reaction would allow the use of a wide variety of azido- or ethynyl-functionalized molecules to be used in the fabrication of other multilayer assemblies. We are currently examining other molecular building blocks that may lead to smoother films with a higher degree of order.

## ■ EXPERIMENTAL SECTION

**Materials.** Solvents, ACS reagent grade or better, were purchased from Sigma Aldrich or Fisher Scientific and used as received. Dry toluene was purged with nitrogen and stored over molecular sieves before use. Sodium ascorbate (Aldrich) and 4,4'-diazido-2,2'-stilbenedisulfonic acid disodium salt tetrahydrate (3) (Fluka) were used as received. 11-Azidoundecyltrimethoxysilane,<sup>90</sup> Zn(II) 5,10,15,20-tetra(4-ethynylphenyl)porphyrin (1),<sup>91</sup> tris-(benzyltriazolylmethyl)amine (TBTA),<sup>92</sup> and 1,3,5-tris(azidomethyl)benzene (2)<sup>93</sup> were synthesized according to literature methods. Si(100) wafers (p-type, 1–100 ohm/cm) were obtained from University Wafer.

Azido-SAM Formation on Silicon. Prior to use, silicon wafers were washed with solvents, last DI water and then cleaned in a piranha solution for at about 30 min (piranha = 3:1 v/v sulfuric acid to 30% hydrogen peroxide, CAUTION! Reacts violently with organics!). The silicon wafers were then rinsed with copious amounts of DI water, dried under a stream of nitrogen, and placed in a Schlenk flask at a pressure of 10<sup>-4</sup> Torr to remove residual water. The slides were then submerged in a solution of approximately 1 mM 11-azidoundecyltrimethoxysilane in anhydrous toluene. The reaction vessel was then heated at 60–70 °C overnight. After cooling to room temperature, the slides were removed and sonicated in toluene for 5 min, after which they were washed with acetone, DCM, ethanol, and water, and then dried in a stream of nitrogen. Slides were then placed in an oven at 75 °C for at least 4 h.

**Multilayer Fabrication.** Ethynyl-porphyrin layers: A solution of DMSO, containing <2% water, consisting of 1.3 mM 1, 0.325 mM CuSO<sub>4</sub>, 0.358 mM TBTA, and 0.48 mM sodium ascorbate was placed in contact with one side of a SAM functionalized silicon sample. After 5 min the slide was washed with acetone, dichloromethane, ethanol, and water. Azidolinker layer: DMSO solution, containing <8% water, was used as described above consisting of 2.2 mM of the selected azide functionalized linker molecule (2 or 3), 4.4 mM CuSO<sub>4</sub>, 4.8 mM TBTA, and 8.9 mM sodium ascorbate.

**Electronic Specular Reflectance Spectroscopy.** Electronic reflectance spectra were taken on a Perkin-Elmer Lamda 950 spectrometer using a near normal specular reflectance accessory (6° from surface normal). A background spectrum of an 11-azidoundecyltrimethoxysilane SAM functionalized Si(100) substrate was subtracted from each spectrum.

**X-ray Specular Reflectivity.** X-ray specular reflectivity profiles were obtained on a Bruker D8 Discover with a 2-circle Theta/2Theta goniometer and a centric Eulerian cradle. The sealed tube copper X-ray source (Cu Kα λ = 1.54 Å) was operated at 40 kV followed by a 40 mm Gobel collimating mirror and a 4 position rotary absorber for incident beam with attenuation of approximately 1:1, 1:10, 1:100, and 1:1000. Slits of 1.0 mm and 0.2 mm were used before and after the rotary absorber respectively. Samples were mounted on a 5 in. vacuum chuck. A knife edge was used for some samples but was found not to affect the resulting reflectivity spectrum beyond the critical angle. Step sizes and dwell times varied from sample to sample depending on the fringe patterns and desired signal-to-noise.

Simulated XRR curves were generated using the LEPTOS software from Bruker with a three-layer model consisting of a layer of SiO<sub>2</sub>, SAM (organic), and porphyrin multilayer (organic) on top of a Si(100) substrate. A genetic algorithm was used to create fit curves and repetitive fits were performed until the fit curve reached a constant value for each parameter. Good fitting results were obtained with the density of the

SiO<sub>2</sub> set to 2.20 g/cm<sup>3</sup> and the SAM layer density at 0.85 g/cm<sup>3</sup>.<sup>67,94,95</sup> In general the variables that were fit were constrained to values that were within reason, and the fitting was performed on the reflectivity curve from approximately 2θ = 0.4° (just below the critical angle) to a region where the fringe patterns could no longer be discerned. For the final fit curves (reported) the following parameters were fit: SiO<sub>2</sub> roughness, SAM roughness, and multilayer thickness, roughness, and density. The Si roughness, SiO<sub>2</sub> thickness, and SAM thickness were assumed to be constant across a sample batch and were fixed to values deemed appropriate based on initial fitting results. In general the roughness of silicon was about 0.3 nm, the thickness of SiO<sub>2</sub> was 1–2 nm, and the value used for the SAM thickness was kept at 1.8 nm for all samples. The value of 1.8 nm used for the SAM thickness is roughly in agreement with reported values for similar length SAMs on silicon (without terminal azides),<sup>94</sup> as well as the value obtained from XRR fitting of a sample functionalized with a SAM only (see the Supporting Information). It is important to note that when the SAM thicknesses were manually adjusted (higher or lower) then the resulting multilayer thickness (after fitting) would adjust accordingly such that the total film thickness (SAM + multilayer) remained nearly identical. Mass densities determined by LEPTOS were given for a pure carbon film and converted to electron densities by the following eq 5<sup>67</sup>

$$\rho_m = \frac{\rho_{el} A}{N_A Z} \quad (5)$$

The reported densities were converted back to mass densities using eq 6<sup>96</sup>

$$\rho_m = \frac{\rho_{el} \sum A_j c_j}{N_A \sum Z_j} \quad (6)$$

This method accounts for the fact that the electron density for our films is not necessarily the same as carbon. Formulas for oligomers of porphyrin and the two different linkers were used to calculate the reported mass density.

**Spectroscopic Ellipsometry.** Spectroscopic ellipsometry measurements were performed on the same samples following analysis by XRR using a J. A. Woollam VASE Ellipsometer, model M-44. Δ and Ψ data were acquired over the full spectroscopic range of the ellipsometer (410 to 741.5 nm, 44 data points) at incident angles of 65°, 70°, and 75°. The data were fit using the WVASE software package from J. A. Woollam using a three layer model consisting of the Si(100) substrate layer, a thin SiO<sub>2</sub> layer, and the Cauchy layer that describes the multilayer film including the 11-azidoundecyltrimethoxysiloxane SAM. The SiO<sub>2</sub> thickness for each sample set was determined from an unfunctionalized Si(100) substrate cleaned in the same manner as the multilayer functionalized samples. To determine the multilayer film thicknesses, the Cauchy dispersion model was employed over the nonabsorbing range of the porphyrin (where the extinction coefficient  $k(\lambda) \cong 0$ , 673.9 to 741.5 nm, 10 data points) to determine  $n(\lambda)$  via eq 3. Optical modeling of the real and complex dielectric functions of the thicker multilayer samples films were accomplished by generating several Lorentz oscillator to reproduce the absorption profile of the film. This method imposes Kramers–Kronig consistency (via eq 4) between  $n(\lambda)$  and  $k(\lambda)$  across the wavelength range being analyzed.<sup>66</sup> An initial guess of  $k(\lambda)$  for the multilayer films was generated from a point-by-point fit of data following a determination of the film thickness by the Cauchy model. During the optical modeling of the spectroscopic ellipsometry data, the film thickness was held constant and only  $n(\lambda)$  and  $k(\lambda)$  for the multilayer film were fitted.

**Atomic Force Microscopy.** Surface topology was analyzed and imaged using atomic force microscopy in tapping mode. Samples were pretreated by washing with MQ water and drying with a stream of nitrogen, and then keeping the sample under vacuum for a few hours.

Atomic force microscopy (AFM) images were recorded using a Digital Instruments Multimode IIIa operated in tapping mode. The cantilevers employed herein were ultrasharp silicon probes (MikroMasch) with a tip radius of  $\sim 10$  nm and a resonant frequency of  $\sim 160$  kHz. Roughness values were obtained using n-Surf image processing software.

**X-ray Photoelectron Spectroscopy.** XPS measurements were made on a Phi 5000 Versa Probe from Physical Electronics with an Al K $\alpha$  X-ray source and a hemispherical analyzer with the analytical chamber at a vacuum level  $\leq 5 \times 10^{-7}$  Pa. Spectra were collected with an angle of incidence of  $45^\circ$ . All spectra were referenced to the C 1s peak at 284.5 eV. Survey scans were acquired at 1 eV data intervals with a band-pass energy of 117.4 eV, while the high resolution scans for Cu and Zn were taken at 0.1 eV intervals and a band-pass energy of 23.5 eV. All high resolution spectra were fit using the Peak Fit software suite with a Gaussian + Lorentzian peak shape after a linear background subtraction. Peak areas for the Cu 2p<sub>3/2</sub> and Zn 2p<sub>3/2</sub> peaks were used to determine the percent copper in the films with the following atomic sensitivity factors: 5.321 for Cu 2p<sub>3/2</sub> and 3.726 for Zn 2p<sub>3/2</sub>.<sup>87,88</sup>

**Computational Details.** Geometry optimizations for the porphyrin-azido-linker constructs were carried out using DFT as implemented in Gaussian 03, revision E.01.<sup>97</sup> Becke's three-parameter hybrid functional<sup>98–101</sup> with the LYP correlation functional<sup>102</sup> (B3LYP) was used with the 6-31++g\*\* basis set for S and O and 3-21 g for C, N, H, and Zn. Both porphyrin models were optimized under the S<sub>4</sub> point group.

## ■ ASSOCIATED CONTENT

**§ Supporting Information.** Table summarizing the physical properties of all multilayer samples used in this study, UV-visible specular reflectance spectra for the multilayers of **1** and **2** grown on Si(100), XRR scans for the stilbene B and mesitylene A and B samples sets, spectroscopic ellipsometry from the stilbene A sample set, XPS survey and high resolution scans of multilayers of **1** and **2** and **1** and **3** grown on Si(100), and the complete ref 97. This material is available free of charge via the Internet at <http://pubs.acs.org>.

## ■ AUTHOR INFORMATION

### Corresponding Author

\*E-mail: dinolp@rpi.edu.

## ■ ACKNOWLEDGMENT

We gratefully acknowledge Prof. Gow-Ching Wang and Joseph Palazzo for assistance in collecting and analyzing the XPS spectra of our multilayer films. P.K.B.P acknowledges a Wiseman Family Fellowship from Rensselaer Polytechnic Institute. This work was supported by Rensselaer Polytechnic Institute through new faculty start-up funds.

## ■ REFERENCES

- (1) George, S. M.; Yoon, B.; Dameron, A. A. *Acc. Chem. Res.* **2009**, *42*, 498–508.
- (2) Xi, Z.; Jiacong, S. *Adv. Mater.* **1999**, *11*, 1139–1143.
- (3) Ariga, K.; Hill, J. P.; Ji, Q. *Phys. Chem. Chem. Phys.* **2007**, *2319–2340*.
- (4) Decher, G.; Hong, J. D. *Makromol. Chem. Macromol. Symp.* **1991**, *46*, 321–327.
- (5) Decher, G.; Hong, J. D. *Ber. Bunsen-Ges. Phys. Chem.* **1991**, *95*, 1430–1434.
- (6) Decher, G.; Hong, J. D.; Schmitt, J. *Thin Solid Films* **1992**, *210*, 831–835.
- (7) Decher, G. *Science* **1997**, *277*, 1232–1237.
- (8) Netzer, L.; Sagiv, J. *J. Am. Chem. Soc.* **1983**, *105*, 674–676.
- (9) Pomerantz, M.; Segmüller, A.; Netzer, L.; Sagiv, J. *Thin Solid Films* **1985**, *132*, 153–162.
- (10) Lee, H.; Kepley, L. J.; Hong, H. G.; Akhter, S.; Mallouk, T. E. *J. Phys. Chem.* **1988**, *92*, 2597–2601.
- (11) Lee, H.; Kepley, L. J.; Hong, H. G.; Mallouk, T. E. *J. Am. Chem. Soc.* **1988**, *110*, 618–620.
- (12) Cao, G.; Hong, H. G.; Mallouk, T. E. *Acc. Chem. Res.* **2002**, *25*, 420–427.
- (13) Yang, H. C.; Aoki, K.; Hong, H. G.; Sackett, D. D.; Arendt, M. F.; Yau, S. L.; Bell, C. M.; Mallouk, T. E. *J. Am. Chem. Soc.* **2002**, *115*, 11855–11862.
- (14) Lee, H.; Kepley, L. J.; Hong, H. G.; Akhter, S.; Mallouk, T. E. *J. Phys. Chem.* **2002**, *92*, 2597–2601.
- (15) Tillman, N.; Ulman, A.; Penner, T. L. *Langmuir* **1989**, *5*, 101–111.
- (16) Evmenenko, G.; Boom, M. E. v. d.; Kmetko, J.; Dugan, S. W.; Marks, T. J.; Dutta, P. *J. Chem. Phys.* **2001**, *115*, 6722–6727.
- (17) Facchetti, A.; Abbotto, A.; Beverina, L.; van der Boom, M. E.; Dutta, P.; Evmenenko, G.; Pagan, G. A.; Marks, T. J. *Chem. Mater.* **2003**, *15*, 1064–1072.
- (18) Li, D.; Ratner, M. A.; Marks, T. J.; Zhang, C.; Yang, J.; Wong, G. K. *J. Am. Chem. Soc.* **1990**, *112*, 7389–7390.
- (19) Lin, W.; Lin, W.; Wong, G. K.; Marks, T. J. *J. Am. Chem. Soc.* **1996**, *118*, 8034–8042.
- (20) van der Boom, M. E.; Richter, A. G.; Malinsky, J. E.; Lee, P. A.; Armstrong, N. R.; Dutta, P.; Marks, T. J. *Chem. Mater.* **2000**, *13*, 15–17.
- (21) van der Boom, M. E.; Zhu, P.; Evmenenko, G.; Malinsky, J. E.; Lin, W.; Dutta, P.; Marks, T. J. *Langmuir* **2002**, *18*, 3704–3707.
- (22) Neff, G. A.; Helfrich, M. R.; Clifton, M. C.; Page, C. *J. Chem. Mater.* **2000**, *12*, 2363–2371.
- (23) Zeppenfeld, A. C.; Fiddler, S. L.; Ham, W. K.; Klopfenstein, B. J.; Page, C. *J. Am. Chem. Soc.* **1994**, *116*, 9158–9165.
- (24) Katz, H. E.; Scheller, G.; Putvinski, T. M.; Schilling, M. L.; Wilson, W. L.; Chidsey, C. E. D. *Science* **1991**, *254*, 1485–1487.
- (25) Splan, K. E.; Hupp, J. T. *Langmuir* **2004**, *20*, 10560–10566.
- (26) Massari, A. M.; Gurney, R. W.; Wightman, M. D.; Huang, C. H. K.; Nguyen, S. B. T.; Hupp, J. T. *Polyhedron* **2003**, *22*, 3065–3072.
- (27) Kohli, P.; Blanchard, G. J. *Langmuir* **2000**, *16*, 4655–4661.
- (28) Li, Y.-h.; Wang, D.; Burak, J. M. *Langmuir* **2009**.
- (29) Schmidt, I.; Jiao, J.; Thamyongkit, P.; Sharada, D. S.; Bocian, D. F.; Lindsey, J. S. *J. Org. Chem.* **2006**, *71*, 3033–3050.
- (30) Jiao, J.; Anariba, F.; Tiznado, H.; Schmidt, I.; Lindsey, J. S.; Zaera, F.; Bocian, D. F. *J. Am. Chem. Soc.* **2006**, *128*, 6965–6974.
- (31) Li, D.; Buscher, C. T.; Swanson, B. I. *Chem. Mater.* **1994**, *6*, 803–810.
- (32) Altman, M.; Shukla, A. D.; Zubkov, T.; Evmenenko, G.; Dutta, P.; van der Boom, M. E. *J. Am. Chem. Soc.* **2006**, *128*, 7374–7382.
- (33) Altman, M.; Zenkina, O.; Evmenenko, G.; Dutta, P.; van der Boom, M. E. *J. Am. Chem. Soc.* **2008**, *130*, 5040–5041.
- (34) Motiei, L.; Altman, M.; Gupta, T.; Lupo, F.; Gulino, A.; Evmenenko, G.; Dutta, P.; van der Boom, M. E. *J. Am. Chem. Soc.* **2008**, *130*, 8913–8915.
- (35) Altman, M.; Zenkina, O. V.; Ichiki, T.; Iron, M. A.; Evmenenko, G.; Dutta, P.; van der Boom, M. E. *Chem. Mater.* **2009**, *21*, 4676–4684.
- (36) Palomaki, P. K. B.; Dinolfo, P. H. *Langmuir* **2010**, *26*, 9677–9685.
- (37) Rostovtsev, V. V.; Green, L. G.; Fokin, V. V.; Sharpless, K. B. *Angew. Chem., Int. Ed.* **2002**, *41*, 2596–2599.
- (38) Tornoe, C. W.; Christensen, C.; Meldal, M. J. *Org. Chem.* **2002**, *67*, 3057–3064.
- (39) Sumerlin, B. S.; Vogt, A. P. *Macromolecules* **2010**, *43*, 1–13.
- (40) Meldal, M.; Tornoe, C. W. *Chem. Rev.* **2008**, *108*, 2952–3015.
- (41) Collman, J. P.; Devaraj, N. K.; Chidsey, C. E. D. *Langmuir* **2004**, *20*, 1051–1053.
- (42) Collman, J. P.; Devaraj, N. K.; Eberspacher, T. P. A.; Chidsey, C. E. D. *Langmuir* **2006**, *22*, 2457–2464.

- (43) Devaraj, N. K.; Decreau, R. A.; Ebina, W.; Collman, J. P.; Chidsey, C. E. D. *J. Phys. Chem. B* **2006**, *110*, 15955–15962.
- (44) Devaraj, N. K.; Dinolfo, P. H.; Chidsey, C. E. D.; Collman, J. P. *J. Am. Chem. Soc.* **2006**, *128*, 1794–1795.
- (45) Devaraj, N. K.; Miller, G. P.; Ebina, W.; Kakaradov, B.; Collman, J. P.; Kool, E. T.; Chidsey, C. E. D. *J. Am. Chem. Soc.* **2005**, *127*, 8600–8601.
- (46) Prakash, S.; Long, T. M.; Selby, J. C.; Moore, J. S.; Shannon, M. A. *Anal. Chem.* **2006**, *79*, 1661–1667.
- (47) Lummerstorfer, T.; Hoffmann, H. *J. Phys. Chem. B* **2004**, *108*, 3963–3966.
- (48) Ku, S.-Y.; Wong, K.-T.; Bard, A. J. *J. Am. Chem. Soc.* **2008**, *130*, 2392–2393.
- (49) Such, G. K.; Quinn, J. F.; Quinn, A.; Tjipto, E.; Caruso, F. *J. Am. Chem. Soc.* **2006**, *128*, 9318–9319.
- (50) Bergbreiter, D. E.; Chance, B. S. *Macromolecules* **2007**, *40*, 5337–5343.
- (51) Rydzek, G.; Thomann, J.-S.; Ben Aumeur, N.; Jierry, L.; Me sini, P.; Ponche, A.; Contal, C.; El Haitami, A. E.; Voegel, J.-C.; Senger, B.; Schaaf, P.; Frisch, B. t.; Boulmedais, F. *Langmuir* **2009**, *26*, 2816–2824.
- (52) Vestberg, R.; Malkoch, M.; Kade, M.; Wu, P.; Fokin, V. V.; Sharpless, K. B.; Drockenmuller, E.; Hawker, C. J. *J. Polym. Sci., Part A: Polym. Chem.* **2007**, *45*, 2835–2846.
- (53) Kadish, K.; Smith, K. M.; Guillard, R. *The Porphyrin Handbook*; Academic Press: New York, 1999.
- (54) Wasielewski, M. R. *Chem. Rev.* **1992**, *92*, 435–461.
- (55) Abdelrazzaq, F. B.; Kwong, R. C.; Thompson, M. E. *J. Am. Chem. Soc.* **2002**, *124*, 4796–4803.
- (56) Yamada, H.; Imahori, H.; Nishimura, Y.; Yamazaki, I.; Ahn, T. K.; Kim, S. K.; Kim, D.; Fukuzumi, S. *J. Am. Chem. Soc.* **2003**, *125*, 9129–9139.
- (57) Tachibana, Y.; Haque, S. A.; Mercer, I. P.; Durrant, J. R.; Klug, D. R. *J. Phys. Chem. B* **2000**, *104*, 1198–1205.
- (58) Cherian, S.; Wamser, C. C. *J. Phys. Chem. B* **2000**, *104*, 3624–3629.
- (59) Odobel, F.; Blart, E.; Lagree, M.; Villieras, M.; Boujtita, H.; El Murr, N.; Caramori, S.; Alberto Bignozzi, C. *J. Mater. Chem.* **2003**, *13*, 502–510.
- (60) Lee, W. W.-S.; Wong, K.-Y.; Li, X.-M.; Leung, Y.-B.; Chan, C.-S.; Chan, K. S. *J. Mater. Chem.* **1993**, *3*, 1031–1035.
- (61) Rakow, N. A.; Suslick, K. S. *Nature* **2000**, *406*, 710–713.
- (62) Smith, V. C.; Batty, S. V.; Richardson, T.; Foster, K. A.; Johnstone, R. A. W.; Sobral, A. J. F. N.; Gonsalves, A. M. D. A. R. *Thin Solid Films* **1996**, *284–285*, 911–914.
- (63) Gonsalves, A. M. d. R.; Pereira, M. M. *J. Mol. Catal. A: Chem.* **1996**, *113*, 209–221.
- (64) Merlau, M. L.; del Pilar Mejia, M.; Nguyen, S. T.; Hupp, J. T. *Angew. Chem., Int. Ed.* **2001**, *40*, 4239–4242.
- (65) Collman, J. P.; Devaraj, N. K.; Decreau, R. A.; Yang, Y.; Yan, Y. L.; Ebina, W.; Eberspacher, T. A.; Chidsey, C. E. D. *Science* **2007**, *315*, 1565–1568.
- (66) Stern, F.; Frederick, S.; David, T. *Solid State Physics*; Academic Press: New York, 1963; Vol. 15, pp 299–408.
- (67) Holz, V.; Pietsch, U.; Baumbach, T. *High-Resolution X-Ray Scattering from Thin Films and Multilayers*; Springer: New York, 1999; Vol. 149.
- (68) Chason, E.; Mayer, T. M. *Crit. Rev. Solid State Mater. Sci.* **1997**, *22*, 1–67.
- (69) Kiessig, H. *Ann. Phys.* **1931**, *10*, 769–788.
- (70) Parratt, L. G. *Phys. Rev.* **1954**, *95*, 359.
- (71) Als-Nielsen, J. *Physica A (Amsterdam)* **1986**, *140A*, 376–89.
- (72) Wasserman, S. R.; Whitesides, G. M.; Tidswell, I. M.; Ocko, B. M.; Pershan, P. S.; Axe, J. D. *J. Am. Chem. Soc.* **1989**, *111*, 5852–5861.
- (73) Geer, R. E.; Stenger, D. A.; Chen, M. S.; Calvert, J. M.; Shashidhar, R.; Jeong, Y. H.; Pershan, P. S. *Langmuir* **1994**, *10*, 1171–1176.
- (74) Geoffrey, D. H.; David, L. A. *J. Polym. Sci., Part B: Polym. Phys.* **1998**, *36*, 1247–1260.
- (75) Toney, M. F.; Mate, C. M.; Pocker, D. *IEEE Trans. Magnet.* **1998**, *34*, 1774–1776.
- (76) See, Y.-K.; Cha, J.; Chang, T.; Ree, M. *Langmuir* **2000**, *16*, 2351–2355.
- (77) Richter, A.; Guico, R.; Wang, J. *Rev. Sci. Instrum.* **2001**, *72*, 3004.
- (78) Rozlosnik, N.; Gerstenberg, M. C.; Larsen, N. B. *Langmuir* **2003**, *19*, 1182–1188.
- (79) Kohli, S.; Rithner, C. D.; Dorhout, P. K.; Dummer, A. M.; Menoni, C. S. *Rev. Sci. Instrum.* **2005**, *76*, 023906.
- (80) Ishizaki, T.; Saito, N.; SunHyung, L.; Ishida, K.; Takai, O. *Langmuir* **2006**, *22*, 9962–9966.
- (81) Li, D.; Lütt, M.; Fitzsimmons, M. R.; Synowicki, R.; Hawley, M. E.; Brown, G. W. *J. Am. Chem. Soc.* **1998**, *120*, 8797–8804.
- (82) Kaschak, D. M.; Lean, J. T.; Waraksa, C. C.; Saupe, G. B.; Usami, H.; Mallouk, T. E. *J. Am. Chem. Soc.* **1999**, *121*, 3435–3445.
- (83) Vuillaume, P. Y.; Glinel, K.; Jonas, A. M.; Laschewsky, A. *Chem. Mater.* **2003**, *15*, 3625–3631.
- (84) Erokhina, S.; Berzina, T.; Cristofolini, L.; Erokhin, V.; Folli, C.; Konovalov, O.; Marino, I.-G.; Fontana, M. P. *Langmuir* **2008**, *24*, 12093–12096.
- (85) Pantelić, N.; Wansapura, C. M.; Heineman, W. R.; Seliskar, C. J. *J. Phys. Chem. B* **2005**, *109*, 13971–13979.
- (86) Azzam, R. M. A.; Bashara, N. M. *Ellipsometry and Polarized Light*; North-Holland Publishing Co.: New York, 1977.
- (87) Meda, L.; Ranghino, G.; Moretti, G.; Cerofolini, G. F. *Surf. Interface Anal.* **2002**, *33*, 516–521.
- (88) Moulder, J. F.; Stickle, W. F.; Sobol, P. E.; Bomben, K. D. *Handbook of X-Ray Photoelectron Spectroscopy*; Physical Electronics: Japan, 1995.
- (89) Ciampi, S.; Böcking, T.; Kilian, K. A.; James, M.; Harper, J. B.; Gooding, J. J. *Langmuir* **2007**, *23*, 9320–9329.
- (90) Fu, Y.-S.; Yu, S. J. *Angew. Chem., Int. Ed.* **2001**, *40*, 437–440.
- (91) Onitsuka, K.; Kitajima, H.; Fujimoto, M.; Iuchi, A.; Takei, F.; Takahashi, S. *Chem. Commun.* **2002**, 2576–2577.
- (92) Chan, T. R.; Hilgraf, R.; Sharpless, K. B.; Fokin, V. V. *Org. Lett.* **2004**, *6*, 2853–2855.
- (93) Song, Y.; Kohlmeir, E. K.; Meade, T. J. *J. Am. Chem. Soc.* **2008**, *130*, 6662–6663.
- (94) Tidswell, I. M.; Ocko, B. M.; Pershan, P. S.; Wasserman, S. R.; Whitesides, G. M.; Axe, J. D. *Phys. Rev. B* **1990**, *41*, 1111.
- (95) del Campo, V.; Cisternas, E.; Taub, H.; Vergara, I.; Corrales, T.; Soza, P.; Colkmann, U. G.; Bai, M.; Wang, S.; Hansen, F. Y.; Mo, H.; Ehrlich, S. N. *Langmuir* **2009**, *25*, 12962–12967.
- (96) van der Lee, A.; Hamon, H.; Holl, Y.; Grohens, Y. *Langmuir* **2001**, *17*, 7664–7669.
- (97) Frisch, M. J.; et al. *Gaussian 03*, revision E.01; Gaussian, Inc.: Wallingford, CT, 2004. See the Supporting Information for the complete reference.
- (98) Becke, A. D. *Phys. Rev. A* **1988**, *38*, 3098–3100.
- (99) Becke, A. D. *J. Chem. Phys.* **1993**, *98*, 1372–1377.
- (100) Becke, A. D. *J. Chem. Phys.* **1993**, *98*, 5648–5652.
- (101) Stephens, P. J.; Devlin, F. J.; Chabalowski, C. F.; Frisch, M. J. *J. Phys. Chem.* **1994**, *98*, 11623–11627.
- (102) Lee, C.; Yang, W.; Parr, R. G. *Phys. Rev. B* **1988**, *37*, 785.